Pharmaceutical Sciences and Drug Design
ISSN: 3062-4428
2023, Volume 3, Page No: 98-116

Available online at: www.galaxypub.co/page/journals

Galaxy Publication

Galaxy Publication

Systems-Based Metabolomics and Network Pharmacology Reveal MAOA-Dependent Anti-Ferroptotic Mechanisms of Curcumin in Acute Kidney Injury

Katerina Dimitrova[1]*, Todor Slavov[1]

[1]Department of Biotechnology, Faculty of Science, Sofia University, Sofia, Bulgaria.

***E-mail** ✉ k.dimitrova.bg@gmail.com

Received: 27 January 2023; **Revised:** 17 April 2023; **Accepted:** 21 April 2023

ABSTRACT

Acute kidney injury (AKI) remains a major global health concern due to its considerable morbidity and mortality. Increasing evidence points to ferroptosis as a dominant pathological process in AKI, and suppression of monoamine oxidase A (MAOA) as well as 5-hydroxytryptamine signaling has been linked to protection against this form of cell death. Curcumin (Cur), the principal polyphenolic constituent of *Curcuma longa*, has shown renal protective activity in AKI models, yet the molecular basis through which it influences ferroptotic pathways has not been clearly defined. This study investigates how Cur modulates ferroptosis during AKI. A folic acid–induced mouse model of AKI and erastin/RSL-3–triggered ferroptosis in HK-2 cells were utilized to evaluate the renoprotective effects of Cur. Nuclear magnetic resonance (NMR) metabolomics combined with network pharmacology was applied to identify metabolic disruptions and potential Cur-related targets. Molecular docking and enzymatic assays were employed to determine Cur's interaction with MAOA.

Cur treatment improved renal function in vivo, evidenced by reduced serum creatinine and blood urea nitrogen levels, and enhanced survival of HK-2 cells undergoing ferroptotic stress in vitro. Mechanistic analyses revealed that Cur mitigates ferroptosis primarily by inhibiting MAOA activity, thereby influencing the metabolic processing of 5-hydroxy-L-tryptophan. These findings suggest, for the first time, that Cur may act as a functional inhibitor of MAOA to counteract ferroptosis in AKI, offering a new mechanistic rationale for its potential therapeutic value.

Keywords: Acute kidney injury, Curcumin, network pharmacology, Metabolomics, Monoamine oxidase A, Ferroptosis

How to Cite This Article: Dimitrova K, Slavov T. Systems-Based Metabolomics and Network Pharmacology Reveal MAOA-Dependent Anti-Ferroptotic Mechanisms of Curcumin in Acute Kidney Injury. Pharm Sci Drug Des. 2023;3:98-116. https://doi.org/10.51847/HSkwD6pl4L

Introduction

Acute kidney injury (AKI) is a common and severe complication among hospitalized patients and is associated with high rates of morbidity and mortality [1]. It is defined by a rapid decline in glomerular filtration accompanied by the accumulation of metabolic by-products such as creatinine and urea nitrogen [2, 3]. Despite its clinical significance, the long-term impact of AKI is frequently underestimated. Episodes of AKI—particularly when occurring together with conditions such as cardiac dysfunction, renal impairment, or sepsis—significantly increase the risk of progression to chronic kidney disease and subsequently elevate mortality [3, 4]. Mechanistic studies have revealed that immune dysregulation, inflammation, oxidative injury, and programmed cell death contribute substantially to AKI pathophysiology [5–7]. Structural injury to renal tubular epithelial cells, including marked apoptosis and necrosis, is a hallmark of AKI-related renal dysfunction [8]. Although AKI is potentially reversible, current treatment options are primarily supportive, and no widely effective mechanism-based therapy is available.

Growing evidence has identified ferroptosis—an iron-dependent, lipid peroxidation–driven form of regulated cell death—as a central contributor to AKI development [9]. The tryptophan-derived metabolite 5-HT has been shown to exert protective effects against ferroptosis, whereas monoamine oxidase A (MAOA) increases susceptibility to

ferroptotic cell death by degrading 5-HT [10]. Several small-molecule ferroptosis inhibitors, including baicalein [11] and silymarin [12], have demonstrated renoprotective properties in AKI models, supporting ferroptosis inhibition as a promising therapeutic strategy.

Natural compounds with low toxicity and multi-target biological activities have attracted significant attention for managing ferroptosis-associated diseases, including AKI [13, 14]. Curcumin (Cur), the major polyphenolic constituent of *Curcuma longa*, is known for its immunomodulatory, antioxidant, anti-inflammatory, and anti-apoptotic functions [15–18]. Extensive research has documented its therapeutic potential across a variety of kidney disorders [19–21], and studies have reported that Cur can improve renal function in AKI by modulating immune responses, suppressing inflammation, reducing oxidative stress, and limiting apoptosis [22–24]. Clinical investigations have further demonstrated its therapeutic relevance in conditions such as cardiovascular disease, diabetes, and cancer [25, 26]. Additionally, Cur has been implicated in mitigating ferroptosis by inhibiting lipoxygenases, modulating mitochondrial oxidative processes, and regulating ferritinophagy [14, 27]. Nevertheless, whether Cur directly influences ferroptosis in AKI remains unclear, and identifying its molecular targets is necessary to advance its therapeutic application.

Metabolomics, a systems biology approach employing comprehensive analytical techniques, enables high-throughput profiling of endogenous metabolites and captures dynamic biochemical changes associated with physiological or pathological states [28–30]. As a reflection of integrated metabolic regulation influenced by genetic and environmental factors—including diet and medication—metabolomics provides valuable insights into pathway alterations linked to disease [28, 31, 32]. Dysregulated metabolism driven by hypoxia and mitochondrial impairment has been strongly associated with AKI [33]. However, metabolomics alone is insufficient to uncover the upstream molecular mechanisms governing these metabolic disturbances.

Network pharmacology, grounded in systems science, supports the identification of key molecular nodes within complex biological networks and facilitates the development of multi-target therapeutic strategies [34]. By modeling interactions among drugs, targets, pathways, and diseases [35], network pharmacology has become an important tool for identifying active constituents, predicting mechanisms of action, and guiding combination drug design [36–38]. Because network pharmacology generates predictions rather than direct biological evidence, experimental validation is essential. Integrating metabolomics with network pharmacology therefore offers a complementary and powerful strategy to uncover both metabolic alterations and upstream regulatory mechanisms associated with Cur's protective effects in AKI.

In this study, we applied a combined metabolomics–network pharmacology approach to investigate the molecular basis of Cur in AKI treatment. Using a folic acid–induced mouse model, we identified Cur-responsive metabolic changes and molecular targets indicating a major role for ferroptosis inhibition in its renoprotective effects. These findings provide new insights into the therapeutic potential of Cur for AKI management.

After a 7-day acclimation period, the animals were divided at random into three experimental sets (N = 10/group): untreated controls, a group receiving FA to induce kidney injury, and a group receiving Cur in addition to FA. Acute kidney injury was triggered through a single intraperitoneal dose of FA (200 mg/kg), following procedures described previously [39]. Control mice were administered an equal volume of saline. Curcumin (100 mg/kg) was given at the onset of FA induction and then repeated three times at 8-hour intervals within the first 24 hours. All animals were euthanized exactly 24 hours after modelling, and blood and renal tissues were collected for downstream measurements.

Assessment of BUN and creatinine

To evaluate renal function, serum BUN and creatinine concentrations were determined for each mouse (N = 10) using protocols established in earlier studies [21, 39]. Blood was left to clot at room temperature for 30–60 minutes, after which it underwent centrifugation at 14,000 g for 15 minutes. The supernatant was transferred to a fresh tube and spun again (14,000 g for 3 minutes) to eliminate remaining cells. Commercial kits from Solarbio Technology Co., Ltd. (Urea Nitrogen/Urea Content Assay Kit, BC1535; Creatinine Content Assay Kit, BC4915) were used according to the manufacturer's instructions.

Histopathological evaluation

Renal tissues were immersed in 4% phosphate-buffered formaldehyde, processed through a dehydration and paraffin-embedding protocol, and sectioned at a thickness of 5 μm. The slices were stained using hematoxylin and

eosin and examined microscopically with an AE31E inverted microscope (Motic, Xiamen, China). For each kidney, five representative fields were imaged.

Preparation of kidney extracts for NMR analysis

Kidney samples (~100 mg; N = 10/group) were extracted using 1.5 mL of a water–chloroform–methanol mixture (2.85:4:4). Tissue homogenization was performed at 65 Hz for 60 seconds. After vortexing for 5 minutes, the mixture was centrifuged at 12,000 g for 15 minutes at 4°C. Methanol in the supernatant was removed by nitrogen evaporation. The aqueous layer was freeze-dried, reconstituted in 600 µL of 50 mM phosphate buffer (0.1 mM TSP, pH 7.4, 100% D2O), and centrifuged again (12,000 g, 4°C, 15 minutes). The clarified solution was transferred to NMR tubes and given a final brief centrifugation at 1,500 g for 5 minutes at 4°C before data acquisition.

NMR measurements and data processing

One-dimensional ^{1}H-NMR spectra were acquired on an 850 MHz Bruker AVANCE III HD instrument (Bruker BioSpin, Ettlingen, Germany) at 25°C using a NOESYGPPR1D pulse program. The acquisition parameters were: spectral width 20 ppm, relaxation delay 4 seconds, and 32 scans. Spectra were corrected for phase and baseline using MestReNova 9.0. TSP at δ 0.00 served as the chemical shift reference. The spectral region from δ 9.5–0.75 was subdivided into 0.001-ppm bins using MATLAB R2014b, normalized to the TSP integral, and the water resonance region (δ 4.85–4.75) was excluded. Metabolite identification was performed with Chenomx NMR Suite 8.3, the Human Metabolome Database (accessed 1 January 2023), and published literature, with assignments confirmed by 2D ^{1}H-^{13}C HSQC spectra.

Multivariate statistics and pathway interpretation

The processed matrix was imported into SIMCA 14.1 (Umetrics, Sweden). Principal component analysis was used to explore inherent clustering patterns, while partial least squares–discriminant analysis was applied to evaluate group discrimination. A 200-iteration permutation test was used to confirm model robustness (R^2 and Q^2). Statistical significance of metabolite differences was determined using IBM SPSS Statistics 22.0 ($p < 0.05$). Pathway analysis and visualization were performed via MetaboAnalyst 5.0 (accessed 1 January 2023), with pathways considered relevant when both the pathway impact value exceeded 1 and the p-value was below 0.05.

Network pharmacology analysis

Cytoscape 3.8.2 (Cytoscape Consortium, San Diego, CA) was used to construct networks connecting metabolites, proteins, and biochemical pathways. AKI-related gene targets were obtained using the keyword “acute kidney injury” from GeneCards, OMIM, TCMSP, and the Therapeutic Target Database. Curcumin-associated targets were retrieved using “Curcumin” as the search term in SwissTargetPrediction, BATMAN-TCM, STITCH 5.0, and ChEMBL. Overlapping entries between Curcumin-related and AKI-related targets were assumed to represent potential therapeutic targets. KEGG and Gene Ontology enrichment analyses were conducted with the ClueGO plugin. Differential metabolites and predicted Cur-AKI targets were combined in Cytoscape, and an integrated network of metabolites, enzymes, pathways, and genes was generated using Metscape.

Molecular docking

Molecular docking was performed using the Schrödinger suite. The 3D structure of Cur (PubChem CID: 969516) was downloaded from the PubChem Compound database (https://www.ncbi.nlm.nih.gov/pccompound) and converted into pdbqt format through the Maestro–LigPrep workflow. Crystal structures of the proteins of interest—monoamine oxidase A (MAOA; PDB ID: 2Z5Y), glutaminase 1 (GLS1; PDB ID: 3VOY), and glutaminase 2 (GLS2; PDB ID: 4BQM)—were retrieved from the RCSB Protein Data Bank (https://www.rcsb.org/). Each protein structure underwent a standard preparation sequence that included optimization of the protonation state, hydrogen-bond assignment, removal of crystallographic waters, and energy minimization.

Binding pockets were predicted using the SiteMap tool, after which the Receptor Grid Generation module was used to define an optimized grid box around the identified pocket. Docking was conducted at the defined active region, and binding stability was further assessed using MM-GBSA calculations. Binding affinity was evaluated

using the extra precision (XP) Gscore and the MM-GBSA ΔGbind values. Visual representations of top-ranked docking poses were produced with PyMOL.

Enzyme activity assay

Renal tissues were processed according to the manufacturer's instructions for the monoamine oxidase activity kit (Solarlbio, CAT: BC0015). Samples (N = 6/group) were homogenized using a 1:1.5 ratio of tissue mass (g) to extraction buffer (mL). Reagents were added sequentially as directed, and absorbance was measured at 360 nm at both 10 seconds and 2 hours using a BioTek microplate reader (Winooski, VT, USA). Enzyme activity values were normalized to tissue weight.

qPCR

Total RNA was isolated with TriZol (Takara, Kyoto, Japan) following the provided protocol. One microgram of RNA (N = 3/group) was reverse-transcribed into cDNA using the ReverTra Ace qPCR RT Master Mix (LabLead, Beijing, China). Gene expression was quantified with SYBR Green Real-time PCR Master Mix (TOYOBO). The cycling protocol consisted of an initial denaturation at 95°C for 10 min, followed by 39 cycles of 95°C for 10 s, 60°C for 30 s, and 95°C for 10 s. Signals were collected using the CFX96 Real-Time System (BIO-RAD). Relative expression was calculated using the $2^{-\Delta\Delta Ct}$ method, with β-actin serving as the internal reference. Primers were obtained from Sangon Biotech (Shanghai, China):

- **MAOA:** 5’-GACCTTGACTGCCAAGATT-3’ / 5’-GATCACAAGGCTTTATTCTA-3’
- **β-actin:** 5’-CTTCCAGCCTTCCTTCCTGG-3’ / 5’-CTGTGTTGGCGTACAGGTCT-3’

Cell culture

Human renal tubular epithelial HK2 cells (ATCC, Manassas, VA, USA) were maintained in high-glucose DMEM (HyClone) containing 10% fetal bovine serum (Biological Industries), 100 μg/mL streptomycin, and 100 IU/mL penicillin (Thermo Fisher Scientific). Cells were cultured at 37°C in a humidified 5% CO_2 incubator.

Cell counting kit-8 assay

HK2 cells were plated in 96-well plates at 5×10^3 cells per well and allowed to attach for 12 hours. After reaching 80–90% confluence, cultures were treated with 2 μM RSL-3 or 2 μM Erastin to trigger ferroptosis. Cells (N = 5/group) were then exposed to Cur at final concentrations of 50, 25, 10, 5, 1, or 0.1 μM for 24 hours. Subsequently, CCK-8 reagent (10% v/v) was added, and absorbance at 450 nm was recorded after 2–4 hours using a POLARstar Omega microplate reader (BMG LABTECH GmbH, Germany).

Lipid peroxidation measurement

Lipid peroxidation levels were quantified using the MDA assay kit (Beijing Solarbio Technology Co., Ltd.) following the provided protocol (N = 5/group). Absorbance was measured at 530 nm with a microplate reader.

Determination of tissue iron levels

Iron concentrations in kidney samples (N = 5/group) were determined using an iron detection kit (Nanjing Jiancheng Bioengineering Institute). Absorbance was recorded at 520 nm using a multi-mode microplate reader.

Statistical analysis

All data are presented as mean ± standard deviation (SD). Statistical comparisons among groups were performed using one-way ANOVA in IBM SPSS Statistics 22.0. Tukey’s test was used when variances were homogeneous, and the Games–Howell test was applied when they were not. Differences were considered statistically significant at $p < 0.05$. Symbols indicate significance: *p<0.05, **p<0.01, ***p<0.001, ****p<0.0001. Graphs were created using GraphPad Prism 8.0.2.

Results and Discussion

Cur administration mitigates FA-induced renal damage in mice

Folic acid–induced AKI is known to resemble clinical manifestations of human AKI, including heightened oxidative stress, inflammatory responses, and extensive tubular injury with subsequent regeneration. To evaluate

the protective effect of Cur in this model, mice were subjected to high-dose FA to induce AKI and were then treated with Cur according to the protocol illustrated in **Figure 1a**.

Mice receiving Cur exhibited markedly lower serum creatinine and blood urea nitrogen concentrations compared with untreated FA-injured mice **(Figures 1b and 1c)**, indicating substantial improvement in renal function. Histopathological evaluation using haematoxylin and eosin staining demonstrated that Cur treatment attenuated the pronounced tubular damage and structural abnormalities observed in the FA group **(Figure 1d)**.

Overall, these findings demonstrate that Cur effectively ameliorates both functional impairment and morphological injury associated with FA-induced AKI.

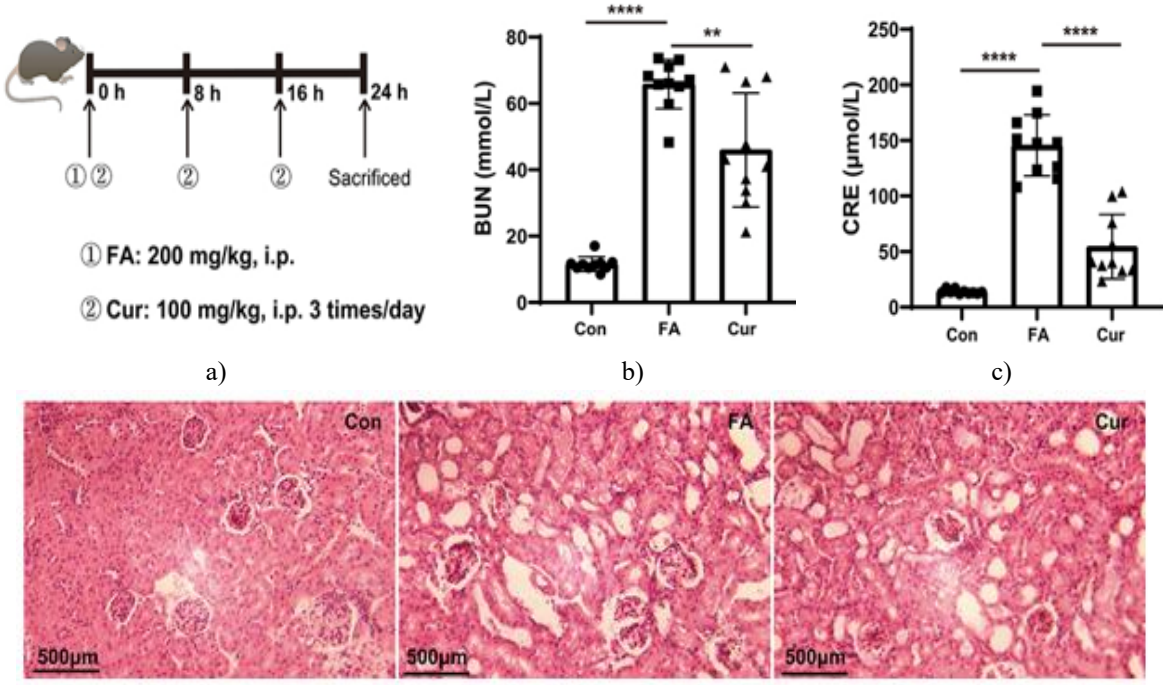

Figure 1. Renoprotective Effects of Curcumin in FA-Induced AKI.

(a) Schematic of the experimental protocol for FA-induced AKI and subsequent Cur administration. (b, c) Serum measurements of blood urea nitrogen (BUN) and creatinine (CRE) demonstrating improved kidney function in Cur-treated mice compared to FA-only mice. (d) Representative haematoxylin-eosin–stained kidney sections showing structural preservation following Cur treatment. Scale bar = 500 μm. Data are expressed as mean ± SD (N = 10). Statistical significance: **p < 0.01; ****p < 0.0001. Each observation represents an independent experiment.

Curcumin alters renal metabolite profiles in AKI

Non-targeted ^{1}H NMR metabolomics of kidney aqueous extracts revealed 41 metabolites across control, FA-treated, and Cur-treated groups. Representative one-dimensional ^{1}H NMR spectra are shown in **Figure 2**. Assignments of metabolite signals were confirmed using 2D ^{1}H–^{13}C HSQC spectra, ensuring accurate identification of the renal metabolic profile changes associated with AKI and Cur treatment.

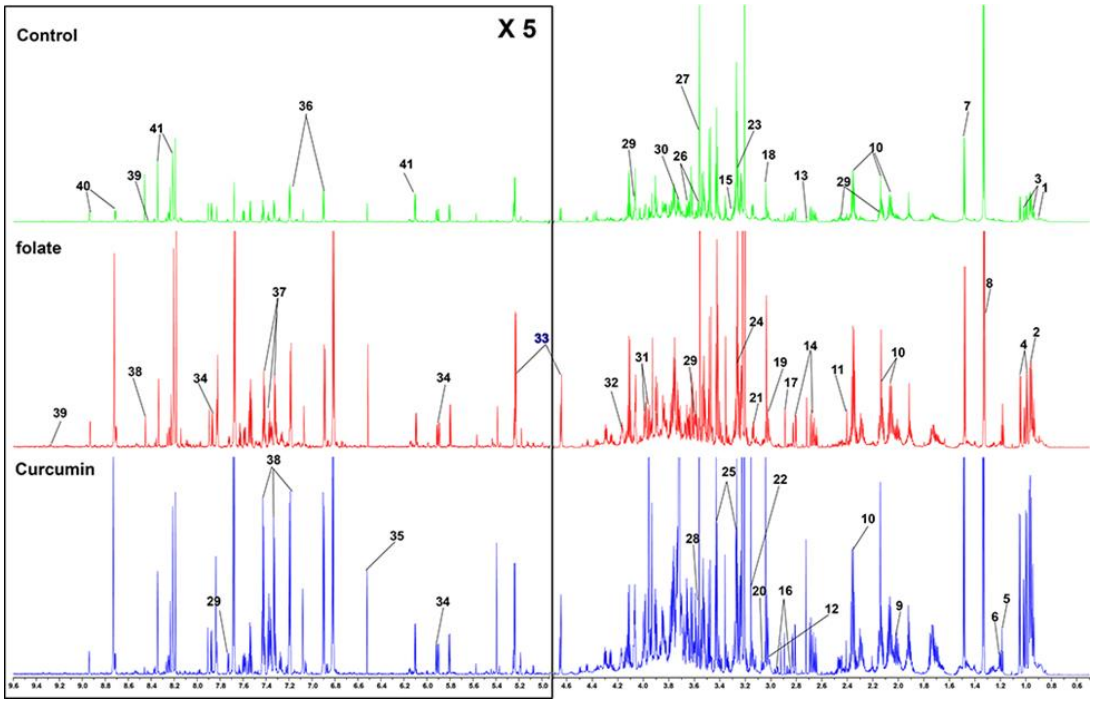

Figure 2. ^{1}H NMR Analysis of Renal Aqueous Extracts

To minimize interference from water signals, the spectral region between δ 4.75–4.85 ppm was excluded. The region from δ 4.85–9.6 ppm was displayed at fivefold the intensity of the δ 0.5–4.75 ppm range to enhance visualization. Peak identities are as follows: 1, Pantothenate; 2, Leucine; 3, Isoleucine; 4, Valine; 5, Ethanol; 6, 3-Hydroxybutyrate; 7, Alanine; 8, Lactate; 9, Proline; 10, Glutamate; 11, Succinate; 12, 5-Hydroxytryptophan; 13, Dimethylamine; 14, Aspartate; 15, Arginine; 16, Glutathione; 17, Trimethylamine; 18, Creatine; 19, Lysine; 20, Ornithine; 21, Ethanolamine; 22, Choline; 23, Trimethylamine N-oxide; 24, Betaine; 25, Taurine; 26, Myo-Inositol; 27, Glycine; 28, Threonine; 29, Tryptophan; 30, Glutamine; 31, Serine; 32, sn-Glycero-3-phosphocholine; 33, Glucose; 34, Uridine; 35, Fumarate; 36, Tyrosine; 37, Phenylalanine; 38, Formate; 39, NAD^{+}; 40, Niacinamide; 41, Inosine.

Curcumin partially restores kidney metabolic profiles in FA-induced AKI

To explore the global metabolic changes associated with FA-induced AKI, we applied unsupervised principal component analysis (PCA) to the ^{1}H NMR spectra of kidney extracts from the three experimental groups. The analysis revealed that samples from the same experimental group clustered together, while clear separation was observed between the FA-treated group and controls, demonstrating profound metabolic disruption caused by AKI **(Figures 3a–3c)**. Interestingly, kidneys from Cur-treated mice occupied an intermediate position between FA-treated and control samples, suggesting that Cur supplementation partially reversed the metabolic perturbations induced by FA. These findings indicate that Cur may exert systemic regulatory effects on renal metabolism, mitigating the biochemical disturbances associated with AKI.

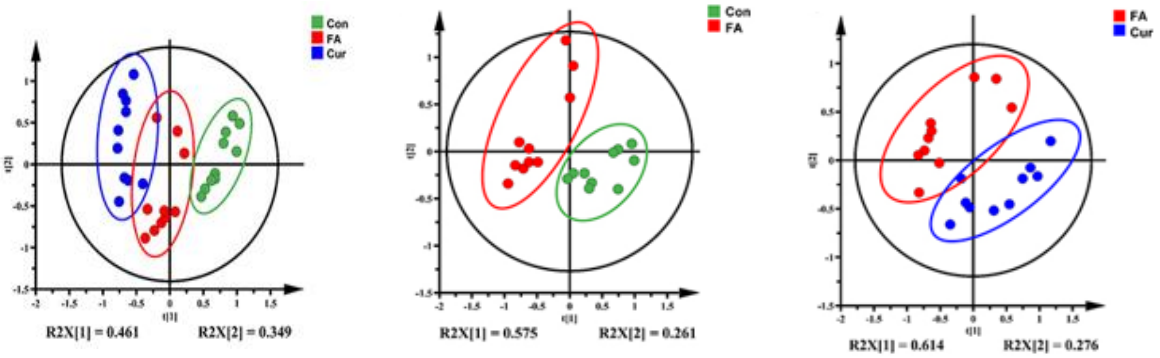

a) b) c)

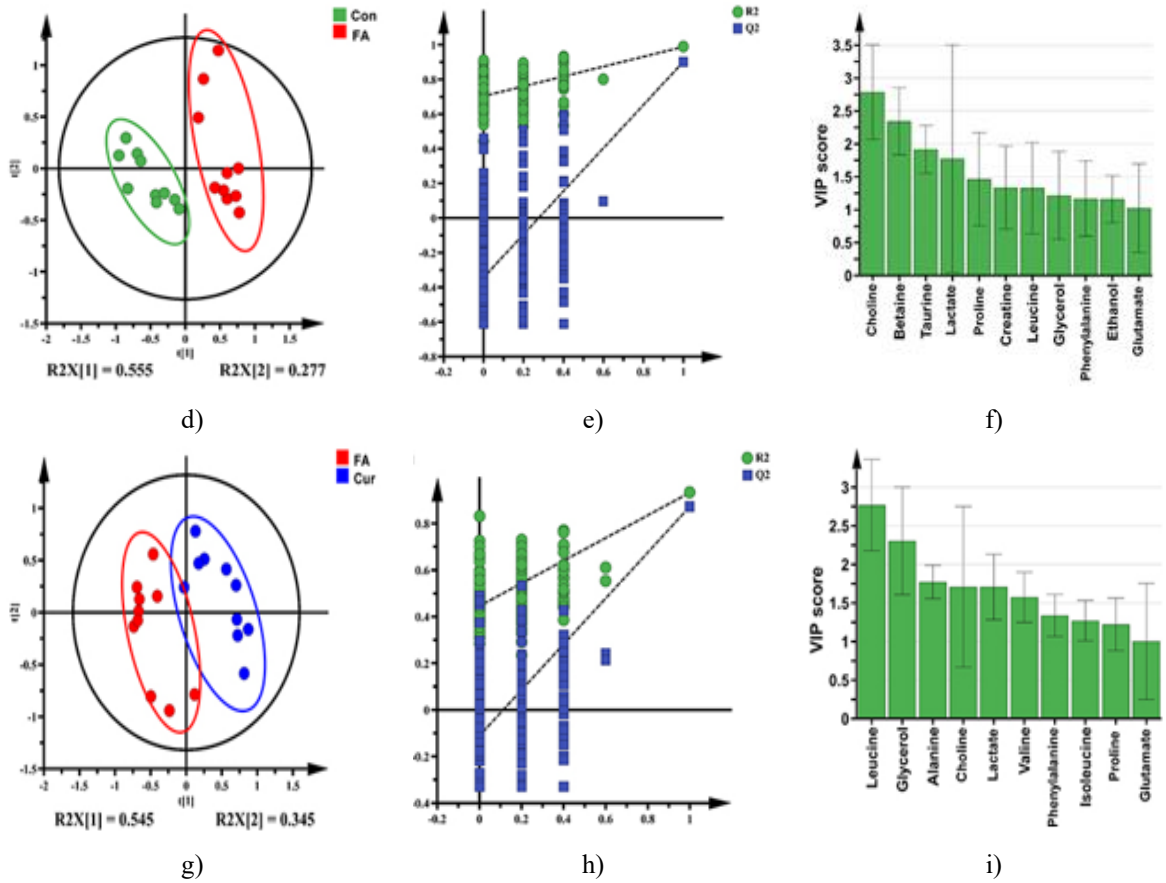

Figure 3. Multivariate Analysis of Kidney Metabolites in Control (Con), Folic Acid (FA), and Curcumin (Cur) Treated Mice (N = 10).
(a–c) PCA score plots showing clustering of the three experimental groups. (d, e) PLS-DA score plots highlighting metabolic separation between FA vs. Con (d) and Cur vs. FA (e). (f, g) Permutation tests validating the PLS-DA models for FA vs. Con. (h, i) Key metabolites (VIP >1) contributing to the separation in FA vs. Con (h) and Cur vs. FA (i).

PLS-DA highlights key metabolic differences and important features

To further resolve group-specific metabolic differences, supervised PLS-DA models were generated. Distinct separation was observed between FA-treated and control kidneys **(Figure 3d)**, as well as between Cur-treated and FA-treated groups **(Figure 3e)**, confirming substantial metabolic perturbations induced by FA and the modulatory effect of Cur. For FA versus control, the model parameters were $R^2X = 0.935$, $R^2Y = 0.988$, and $Q^2 = 0.902$. For Cur versus FA, corresponding values were $R^2X = 0.914$, $R^2Y = 0.933$, and $Q^2 = 0.873$.

The robustness of these models was evaluated using 200 permutation tests **(Figures 3f and 3g)**, indicating strong explanatory (R^2) and predictive (Q^2) power. This confirmed that the PLS-DA models reliably identify metabolites responsible for group separation. From these models, 11 and 10 metabolites were highlighted as important contributors for FA vs. control **(Figure 3h)** and Cur vs. FA **(Figure 3i)**, respectively.

Identification of differential metabolites and key metabolic pathways

Peak integrals of the 41 assigned metabolites were normalized to TSP to determine relative concentrations. Statistical analysis using one-way ANOVA with Tukey's post hoc test ($p < 0.05$) identified 27 significantly altered metabolites between FA-treated and control mice, and 20 metabolites differing between Cur- and FA-treated mice. A heatmap **(Figure 4)** was constructed to visualize group-specific variations in metabolite abundance. Metabolites meeting VIP >1 or $p < 0.05$ criteria were considered characteristic of FA-induced injury or Cur-mediated recovery. Based on these criteria, 30 characteristic metabolites were identified in FA vs. control, and 24 in Cur vs. FA comparisons. Cross-referencing these datasets revealed 19 metabolites that were differentially regulated and likely contribute to the therapeutic effects of Cur in FA-induced AKI **(Table 1)**.

Table 1. The Differential Metabolites in Kidneys of AKI Mice

Metabolites	Mean ± SD			FA vs Con	Cur vs FA	ANOVA	
	Con	FA	Cur			F	P
Leucine	1.221±0.081	1.535±0.275	2.875±0.406	↑***	↑*	89.116	<0.001
Isoleucine	0.277±0.021	0.350±0.069	0.642±0.095	↑*	↑***	74.552	<0.001
Valine	0.469±0.036	0.557±0.101	1.003±0.148	↑*	↑***	70.429	<0.001
Alanine	1.533±0.129	1.347±0.206	1.954±0.317	↓*	↑***	18.482	<0.001
Lactate	5.522±0.418	4.536±1.279	4.147±1.048	ns	ns	4.606	0.019
Proline	0.513±0.057	0.872±0.220	1.178±0.157	↑**	↑***	38.668	<0.001
Glutamate	2.060±0.170	2.297±0.428	2.265±0.389	ns	ns	1.245	0.304
5-Hydroxytryptamine	0.290±0.030	0.261±0.009	0.334±0.052	↓*	↑*	5.714	0.009
Dimethylamine	0.044±0.007	0.179±0.102	0.346±0.056	↑**	↑*	44.093	<0.001
Creatine	0.307±0.049	0.549±0.142	0.788±0.124	↑***	↑***	40.957	<0.001
Lysine	0.210±0.018	0.257±0.049	0.402±0.064	↑*	↑***	41.496	<0.001
Choline	4.776±1.053	3.398±0.942	3.859±0.615	↓**	ns	6.106	0.006
Threonine	0.087±0.009	0.112±0.024	0.159±0.023	↑*	↑**	30.223	<0.001
Tryptophan	1.181±0.336	0.861±0.161	1.629±0.184	↓*	↑***	28.421	<0.001
Glutamine	0.343±0.035	0.300±0.006	0.485±0.063	↓*	↑***	21.715	<0.001
Glucose	0.083±0.014	0.051±0.019	0.036±0.008	↓**	↓*	25.557	<0.001
Fumarate	0.033±0.010	0.057±0.017	0.043±0.007	↑**	↓*	9.631	0.001
Tyrosine	0.147±0.012	0.181±0.035	0.277±0.040	↑*	↑***	42.941	<0.001
Phenylalanine	0.165±0.010	0.404±0.153	0.727±0.108	↑**	↑***	60.228	<0.001

Notes: *Statistical significances (N=10):ns: no statistical significance, $p > 0.05$; *:$p < 0.05$; **:$p < 0.01$; ***:$p < 0.001$. Each repeat was performed as a separate, independent experiment or observation.

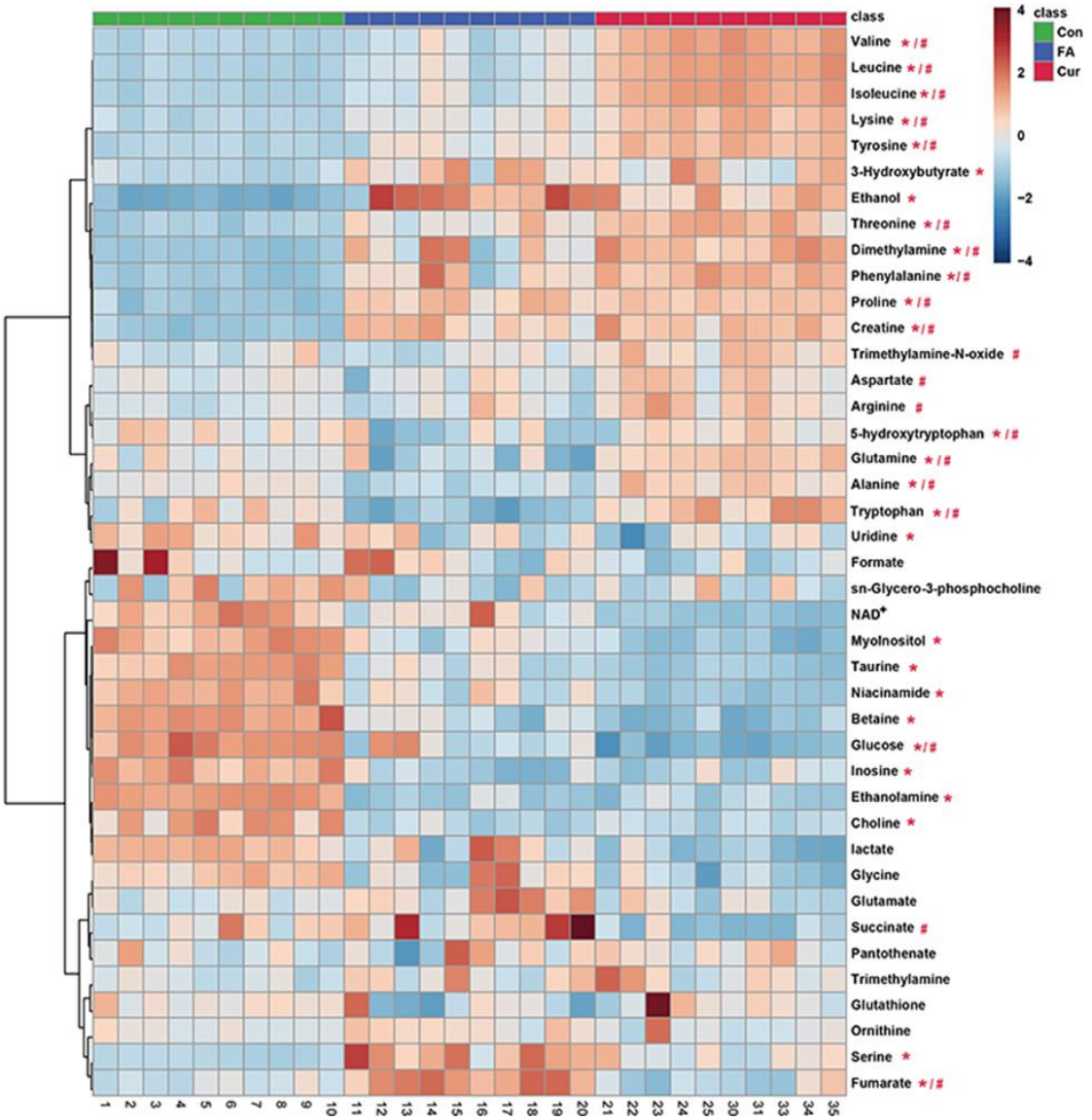

Figure 4. Heatmap of Kidney Metabolite Alterations Across Experimental Groups.
This heatmap displays the relative levels of identified metabolites in kidneys from control (Con), folic acid–treated (FA), and Curcumin-treated (Cur) mice (n = 10). Metabolites significantly altered by FA treatment compared to controls are indicated with "*", while those significantly affected by Cur compared with FA treatment are marked with "#". Each data point represents an independent experiment.

Curcumin influences key metabolic pathways in AKI

To uncover the biochemical pathways affected by FA-induced AKI and modulated by Cur, we performed pathway enrichment analysis using MetaboAnalyst 5.0, with metabolite concentrations serving as input. Pathways were considered significant when their impact values exceeded 0.1 and p-values were below 0.05. This analysis identified nine pathways disrupted in FA-treated kidneys and 11 pathways altered following Cur administration **(Figures 5a and 5b)**.

Several pathways overlapped between the two comparisons, highlighting them as central to AKI progression and Cur's protective effects. These included amino acid–related pathways such as phenylalanine, tyrosine, and tryptophan biosynthesis; phenylalanine metabolism; tryptophan metabolism; tyrosine metabolism; and arginine and proline metabolism. Energy and redox-related pathways such as nicotinate and nicotinamide metabolism, taurine and hypotaurine metabolism, alanine, aspartate, and glutamate metabolism, and inositol phosphate metabolism were also implicated. Together, these results indicate that Cur may mitigate renal injury by restoring multiple interrelated metabolic networks disrupted during AKI.

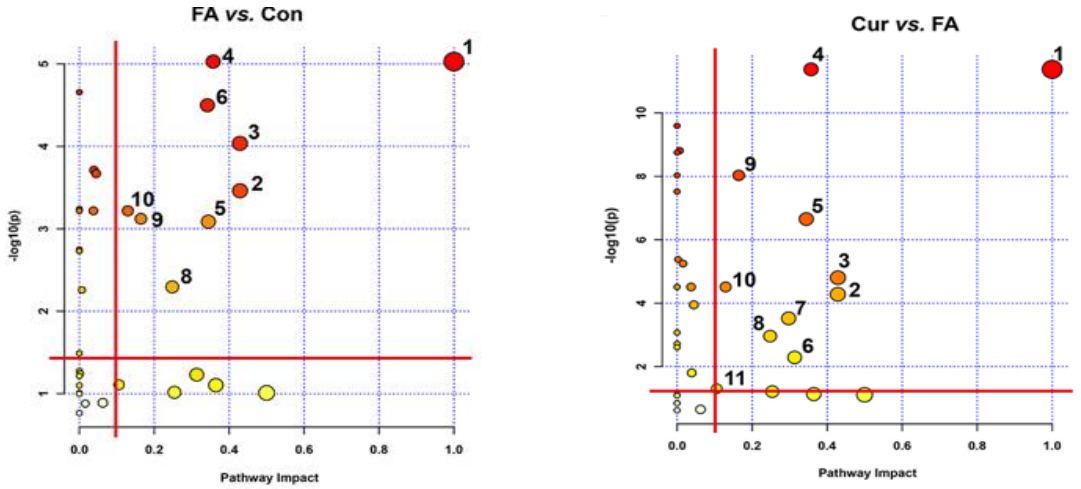

a) b)

Figure 5. Enrichment Analysis of Key Metabolic Pathways.
(a, b) Pathway analysis illustrating the metabolic alterations induced by FA treatment and their modulation following Cur administration. Pathways were considered significant when p-values were below 0.05 and pathway impact values (PIV) exceeded 0.1. Numbers correspond to the following pathways: 1, Phenylalanine, tyrosine, and tryptophan biosynthesis; 2, Nicotinate and nicotinamide metabolism; 3, Taurine and hypotaurine metabolism; 4, Phenylalanine metabolism; 5, Arginine and proline metabolism; 6, Alanine, aspartate, and glutamate metabolism; 7, Glycine, serine, and threonine metabolism; 8, Tryptophan metabolism; 9, Tyrosine metabolism; 10, Inositol phosphate metabolism; 11, Glyoxylate and dicarboxylate metabolism.

Integrative network pharmacology analysis

To gain further insight into the mechanisms underlying Cur's protective effects in AKI, we conducted a network pharmacology study. Initial enrichment analysis using the BATMAN-TCM database identified six pathways that overlapped with those highlighted by metabolomics, including phenylalanine metabolism, glycine/serine/threonine metabolism, tryptophan metabolism, arginine and proline metabolism, tyrosine metabolism, and glyoxylate/dicarboxylate metabolism, supporting the consistency of the metabolomics findings. Next, we compiled potential Cur targets by integrating data from SwissTargetPrediction, STITCH, BATMAN-TCM, and ChEMBL, yielding 162 candidate targets. AKI-related targets were retrieved from TCMSP, TTD, OMIM, and GeneCards databases, resulting in 1788 disease-associated targets. Intersection analysis identified 71 common targets potentially mediating Cur's therapeutic effects, visualized in a Venn diagram **(Figure 6a)**. A compound–target interaction network was subsequently constructed using Cytoscape software to map the relationships between Cur and these candidate AKI targets **(Figure 6b)**.

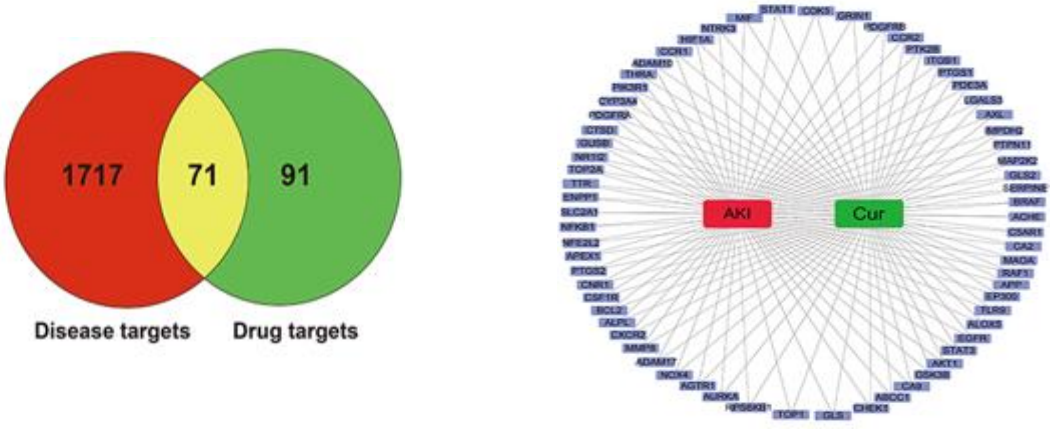

a) b)

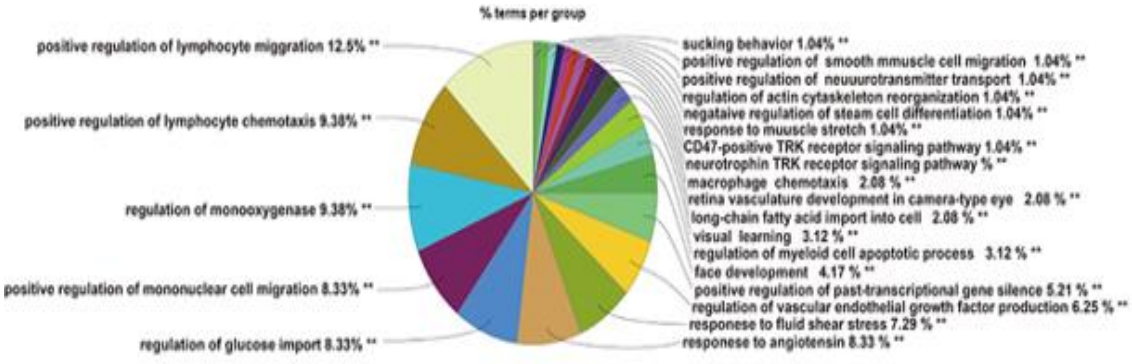

c)

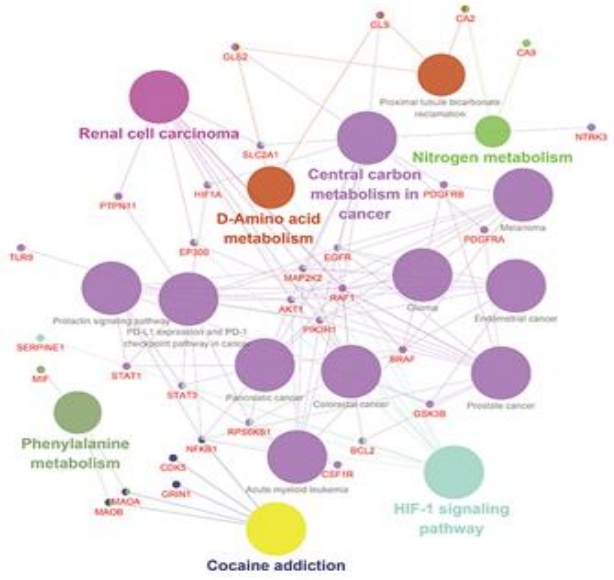

d)

Figure 6. Network Pharmacology Analysis of Curcumin in AKI.
(a) Venn diagram illustrating the overlap between predicted targets of Cur and AKI-associated targets. Green and red areas represent Cur and AKI targets, respectively, while the yellow area shows shared targets. (b) Compound–target interaction network connecting Cur to AKI-related targets. (c) Gene Ontology (GO) enrichment analysis of overlapping targets, performed using ClueGO. (d) KEGG pathway enrichment of the same targets, also analyzed via ClueGO. Only pathways with $p < 0.05$ are shown.

Functional enrichment analysis of curcumin targets

To further investigate the molecular basis of Cur's renoprotective effects, GO and KEGG enrichment analyses were conducted on the 71 overlapping targets identified between Cur and AKI. GO analysis highlighted biological processes such as the positive regulation of lymphocyte migration, lymphocyte chemotaxis, monooxygenase activity regulation, mononuclear cell migration, and glucose import regulation. KEGG pathway enrichment revealed significant involvement of D-amino acid metabolism, central carbon metabolism, nitrogen metabolism, phenylalanine metabolism, renal cell carcinoma–related pathways, cocaine addiction pathways, and the HIF-1α signaling pathway, suggesting that Cur may act through diverse metabolic and signaling networks.

Integration of metabolomics and network pharmacology

To gain a systems-level understanding of how Cur ameliorates AKI, a comprehensive drug–reaction–enzyme–gene network was constructed by combining metabolomics data with network pharmacology results **(Figure 7)**. This integrative approach enabled mapping of upstream targets to downstream metabolites and associated pathways. By correlating the differential metabolites from metabolomics with potential targets from network pharmacology, four key upstream targets were identified: MAOA, GLS1, GLS2, and acetylcholinesterase (ACHE) **(Table 2)**.

These targets were linked to three primary metabolic pathways: alanine, aspartate, and glutamate metabolism; tryptophan metabolism; and choline metabolism. The core metabolites associated with these pathways included L-alanine, L-glutamine, L-glutamate, 5-hydroxy-L-tryptophan (5-HT), L-tryptophan, and choline. While choline metabolism was uniquely identified through network pharmacology, the other two pathways were also prominent in metabolomics analyses. Collectively, these findings suggest that MAOA, GLS1, and GLS2—rather than ACHE—likely play critical roles in mediating Cur's renoprotective effects in FA-induced AKI.

Table 2. The Information of Core Pathways, Metabolites and Metabolites

Metabolic Pathway	Target(s)	Key Metabolites
Alanine, aspartate, and glutamate metabolism	GLS1, GLS2	L-Alanine, L-Glutamine, L-Glutamate
Tryptophan metabolism	MAOA	5-Hydroxy-L-tryptophan, L-Tryptophan
Choline metabolism	ACHE	Choline

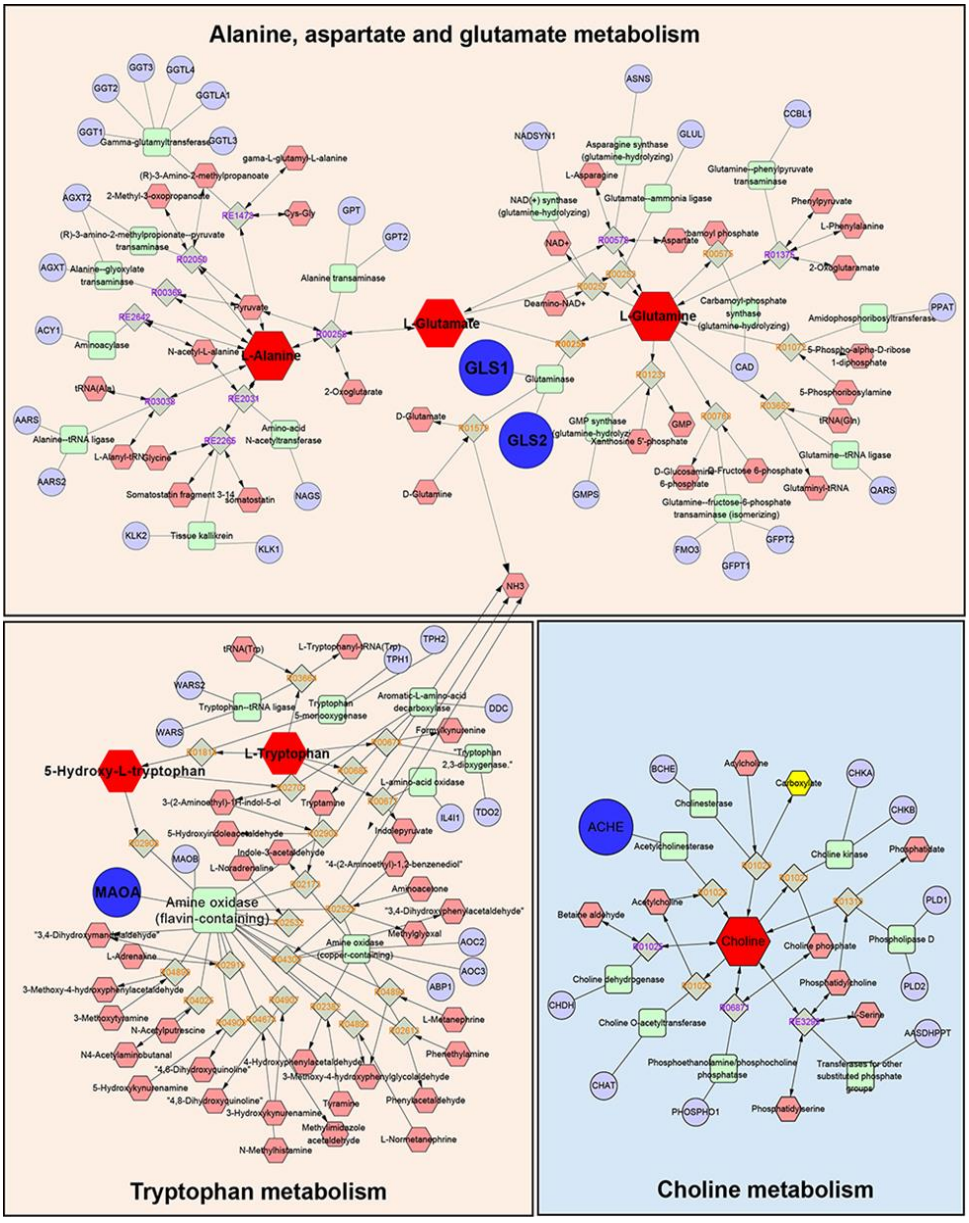

Figure 7. Integrated Interaction Network of Key Genes, Proteins, Pathways, and Metabolites. The network illustrates the relationships among active compounds (red hexagons), reactions (grey diamonds), proteins (green rectangles), and genes (purple circles). Key nodes, including crucial genes, proteins, and metabolites, are enlarged for emphasis. Nodes with a red background represent metabolites that were significantly altered in both FA versus control and Cur versus FA comparisons in the metabolomics analysis.

Molecular docking of curcumin with core targets

To investigate potential molecular interactions between Cur and the identified core targets, molecular docking simulations were performed using Schrödinger software. Core targets included MAOA, GLS1, and GLS2. Docking results are summarized in **Table 1**. Ligand-protein binding was considered favorable if XP GScore was below −6 and MM-GBSA binding free energy (dG Bind) was below −30 kcal/mol.

Table 3. Molecular Docking Results of Curcumin with Core Targets

CID	Compound	Target	PDB ID	XP GScore	MM-GBSA dG Bind (kcal/mol)
969516	Curcumin	MAOA	2Z5Y	−8.973	−55.92
		GLS2	4BQM	−6.023	−56.47
		GLS1	3VOY	−5.197	−38.01

Docking analysis revealed that Cur bound MAOA through hydrogen bonds with GLU43 and ARG51, formed a π-cation interaction with ARG45, and engaged in hydrophobic contacts with TYR402, PRO274, ALA448, MET445, and TYR444 **(Figures 8a and 8d)**. The docking score of −8.973 and binding energy of −55.92 kcal/mol indicate strong and stable binding.

For GLS2, Cur interacted via hydrogen bonds with SER219 and LEU441, along with hydrophobic contacts involving ALA180, ALA181, VAL417, ALA416, and TYR399 **(Figures 8b and 8e)**. The docking score of −6.023 and binding energy of −56.47 kcal/mol suggested good affinity and stable binding.

In the case of GLS1, hydrogen bonds were observed with TYR414, ASN388, LYS289, and LYS245, complemented by hydrophobic interactions with VAL246, ALA247, TYR249, and VAL484 **(Figures 8c and 8f)**. The docking score of −5.197 and binding energy of −38.01 kcal/mol indicated moderate binding affinity and stability.

Overall, these docking studies demonstrate that Cur exhibits strong binding, particularly with MAOA, supporting its potential role in modulating ferroptosis-related pathways in AKI.

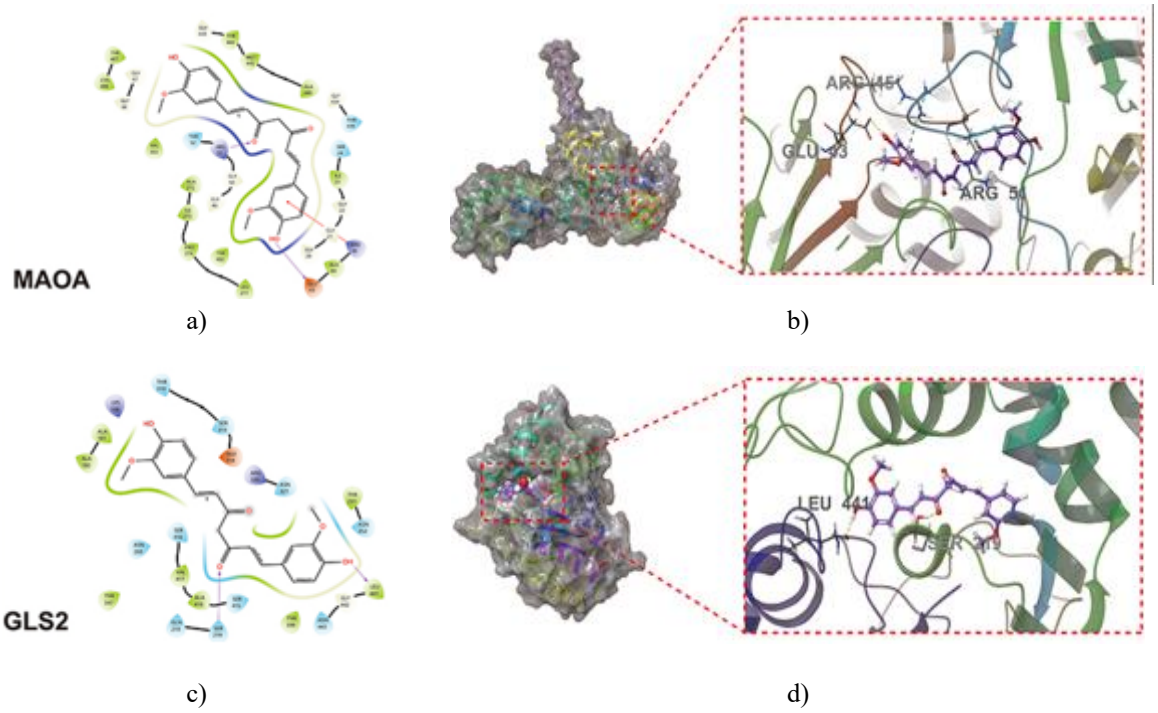

a) b)

c) d)

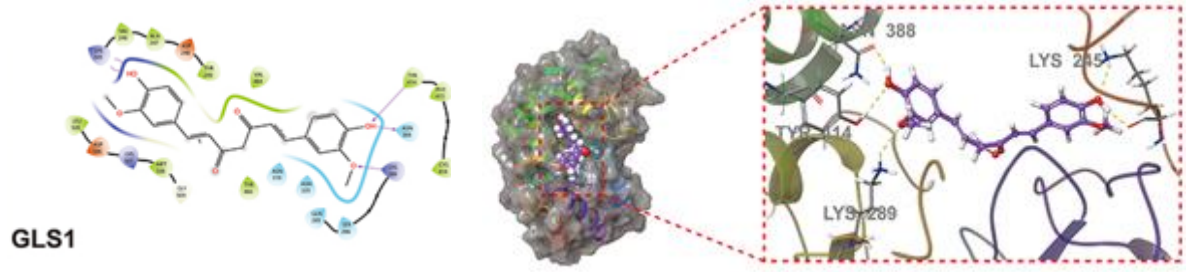

e) f)

Figure 8. Molecular Docking of Curcumin with Core Target Proteins.
(a–c) Two-dimensional (2D) docking interactions between Cur and the key targets monoamine oxidase A (MAOA, a), glutaminase 2 (GLS2, b), and glutaminase 1 (GLS1, c). Purple arrows indicate hydrogen bonds, while red arrows denote π-cation interactions.
(d–f) Three-dimensional (3d) docking representations for Cur bound to MAOA (d), GLS2 (e), and GLS1 (f). Yellow and green dashed lines represent hydrogen-bonding and π-cation interactions, respectively.

Curcumin's renoprotective effects are mediated by MAOA modulation

Given the established link between AKI and MAOA-mediated 5-HT degradation, [40] we evaluated whether MAOA serves as a key target of Cur in AKI treatment. Quantification of MAOA mRNA in kidney tissue revealed a significant upregulation in the FA-treated group compared with controls, whereas Cur administration markedly reduced MAOA expression **(Figure 9a)**. Concordantly, enzymatic activity assays demonstrated a similar trend, with elevated MAOA activity in FA-treated mice that was attenuated by Cur treatment **(Figure 9b)**.
Consistent with these observations, kidney levels of 5-hydroxytryptamine (5-HT) were significantly decreased in the FA-induced AKI group relative to controls, and Cur treatment restored 5-HT levels toward normal **(Figure 9c)**. Collectively, these results indicate that Cur mitigates AKI, at least in part, by downregulating MAOA expression and activity, thereby preserving 5-HT metabolism and contributing to renal protection.

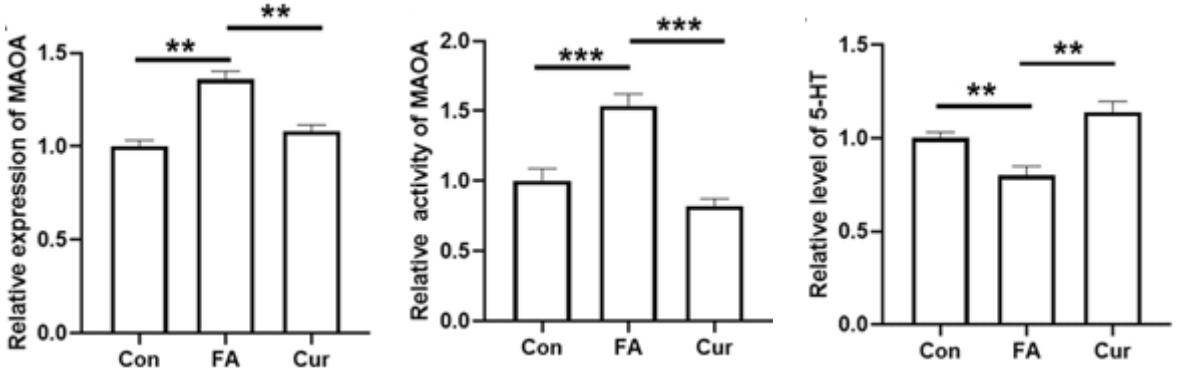

a) b) c)

Figure 9. Curcumin Regulates Renal 5-Hydroxy-L-Tryptophan (5-HT) Metabolism.
(a) Relative MAOA mRNA expression in kidney tissue measured by RT-PCR, normalized to β-actin and expressed as fold change relative to the control (Con) group.
(b) MAOA enzymatic activity in kidney samples, expressed as fold change relative to the Con group.
(c) Relative 5-HT content in kidney tissue, expressed as fold change relative to the Con group. Data are shown as mean ± SD. Statistical significance (N = 6): **p < 0.01; ***p < 0.001. Each experiment was performed independently.

Curcumin exerts anti-ferroptotic effects in AKI

Ferroptosis, characterized by iron-dependent lipid peroxidation, is a critical driver of AKI progression [39]. Inhibition of ferroptosis has been shown to confer renal protection in multiple AKI models [41-43]. Recent studies indicate that the tryptophan metabolite 5-hydroxytryptamine (5-HT) can prevent ferroptotic cell death, while MAOA diminishes this protective effect by degrading 5-HT [44].

Based on these findings, we investigated whether Cur possesses anti-ferroptotic activity. HK2 cells were exposed to ferroptosis inducers RSL-3 or Erastin and subsequently treated with varying concentrations of Cur (1, 5, 10, 25, and 50 μM). Cur treatment effectively reversed ferroptosis in a dose-dependent manner, with near-complete protection observed at 5 μM **(Figures 10a and 10b)**.

In vivo, the lipid peroxidation marker malondialdehyde (MDA) was measured in kidney tissue, and Cur treatment significantly reduced MDA levels **(Figure 10c)**. Kidney iron content, an indicator of ferroptosis, was also decreased following Cur administration **(Figure 10d)**. Collectively, these findings indicate that Cur protects against AKI by inhibiting ferroptosis and reducing iron-dependent oxidative damage.

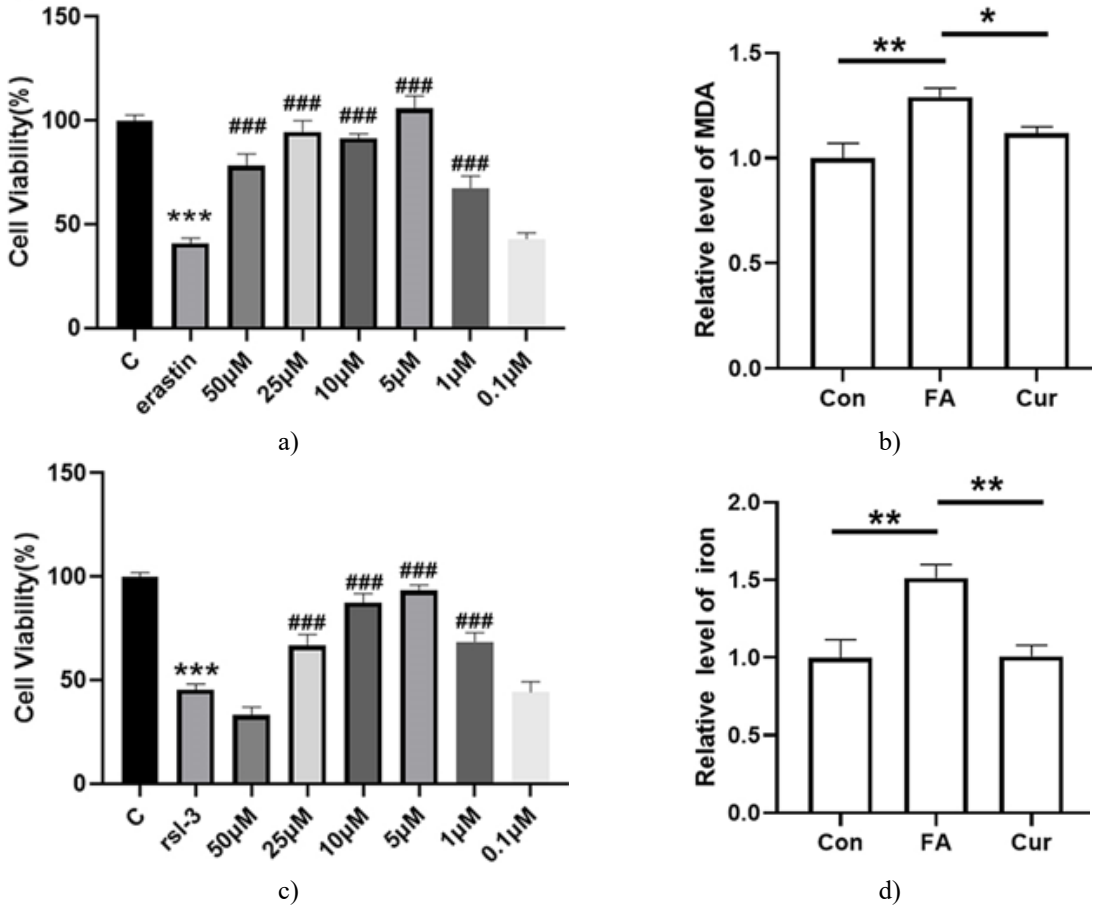

Figure 10. Curcumin Attenuates Ferroptosis in HK2 Cells and Kidney Tissue.

(a, b) Cell viability of HK2 cells treated with 2 μM Erastin (a) or 2 μM RSL-3 (b) to induce ferroptosis, followed by Cur treatment at concentrations of 0.1, 1, 5, 10, 25, and 50 μM for 24 h. Data are shown as mean ± SD (N = 5). ***p < 0.001 indicates significance between control and Erastin or RSL-3 groups; ###p < 0.001 indicates significance between control and Cur-treated groups.

(c) Malondialdehyde (MDA) levels in kidney tissue measured at 530 nm, expressed as fold change relative to the control (Con) group, representing lipid peroxidation (N = 5).

(d) Kidney iron content assessed using a tissue iron assay kit, expressed as fold change relative to the Con group (N = 5). Data are mean ± SD, with significance indicated as *p < 0.05 and **p < 0.01. Each experiment was performed independently.

Acute kidney injury (AKI) results from various physiological and pathological insults leading to impaired renal function [4]. Curcumin (Cur) has emerged as a promising therapeutic agent for kidney disorders due to its diverse pharmacological properties [16, 20, 22]. However, the precise molecular targets and mechanisms through which Cur exerts its effects remain incompletely understood.

In this study, we integrated metabolomics and network pharmacology to uncover the mechanistic basis of Cur in FA-induced AKI. Twelve differential metabolites and their associated pathways were identified as responsive to Cur treatment. Integrative analysis revealed three key protein targets—MAOA, GLS1, and GLS2—two relevant

metabolic pathways—tryptophan metabolism and alanine, aspartate, and glutamate metabolism—and five principal metabolites, including L-alanine, L-glutamine, L-glutamate, 5-HT, and L-tryptophan. Molecular docking further demonstrated strong binding affinity of Cur to MAOA, while in vivo experiments confirmed that Cur modulates 5-HT metabolism via MAOA, suggesting a potential anti-ferroptotic mechanism.

Cur, a natural polyphenol, exhibits broad pharmacological activities, including anticancer effects [44], hepatoprotective benefits [45], and renoprotection [16], while maintaining safety at high doses in humans [46], Previous studies have implicated several mechanisms for Cur in AKI. For example, in glycerol-induced AKI, Cur activates the Keap1/Nrf2 pathway, enhancing antioxidant enzymes such as NQO1, HO-1, and SOD [47], In cisplatin-induced AKI, Cur reduces nitric oxide production by suppressing nitric oxide synthase activity [48] and mitigates inflammatory damage through inhibition of NF-κB signaling [49].

Our metabolomics analysis highlighted 12 differential metabolites and 11 significantly altered pathways **(Table 1 and Figure 5)**, indicating that Cur's renoprotective effects are closely linked to metabolic regulation. However, metabolomics alone cannot fully reveal the upstream regulators and direct interactions among metabolites. By combining metabolomics with network pharmacology, we were able to construct an integrated network connecting targets, pathways, and terminal metabolites, providing a systematic and comprehensive view of the mechanisms through which Cur mitigates AKI.

According to our molecular docking results, MAOA, identified through integration of metabolomics and network pharmacology, displayed the lowest binding energy with Cur **(Table 2)**. MAOA is a mitochondrial enzyme responsible for the oxidative deamination of monoamine neurotransmitters and dietary amines, including 5-HT. Previous research has highlighted a close link between MAOA-mediated 5-HT degradation and the progression of AKI [40]. More recently, 5-HT has been recognized as a potent radical-trapping antioxidant with anti-ferroptotic activity [10]. In our study, Cur treatment inhibited MAOA expression in AKI mice, leading to elevated renal 5-HT levels **(Figure 9)**, suggesting that Cur's renoprotective effect may involve anti-ferroptotic mechanisms.

Regulated cell death pathways—including necroptosis, apoptosis, and ferroptosis—have been implicated in various forms of tissue injury [39]. Ferroptosis is a programmed cell death modality characterized by iron-dependent lipid peroxidation, and evidence indicates it plays a critical role in AKI pathogenesis, as pharmacological inhibition of ferroptosis ameliorates kidney injury in multiple animal models. While Cur has been extensively studied for its anti-ferroptotic effects in cancer [45, 50, 51], its role in AKI has been less explored. In our experiments, Cur effectively suppressed ferroptosis in HK2 cells and reduced the elevated levels of MDA and iron in kidneys of FA-treated mice **(Figure 10)**. These findings support the idea that Cur exerts its anti-ferroptotic effects in AKI by modulating 5-HT metabolism via MAOA, establishing a link between ferroptosis and AKI progression while identifying potential therapeutic targets.

Despite its therapeutic potential, the clinical application of Cur is limited by poor water solubility, low intestinal absorption, and reduced bioavailability [46, 52] Various formulation strategies—including nanoparticles, liposomes, and polymeric micelles—have been developed to improve Cur's pharmacokinetic properties and enhance its therapeutic efficacy [53–55], Additionally, co-administration with bioenhancers such as piperine has shown promise in improving Cur's effectiveness in clinical settings [56] Future development of Cur-based nanoformulations or combination therapies may overcome these limitations and enhance its potential as a clinical intervention for AKI.

Conclusion

This study reaffirms the renoprotective effects of Cur in FA-induced AKI and highlights its ability to mitigate ferroptosis-related renal injury. Using an integrated metabolomics and network pharmacology approach, MAOA was identified as a key molecular target mediating Cur's effects. Further functional validation demonstrated that Cur regulates 5-HT metabolism through MAOA, thereby suppressing ferroptosis. These findings indicate that inhibition of ferroptosis is a critical mechanism by which Cur protects against renal injury, providing a scientific basis for developing Cur and related interventions as potential therapies for ferroptosis-associated diseases, particularly AKI.

Acknowledgments: None

Conflict of Interest: None

Financial Support: This work was supported by Natural Science Foundation of Fujian Province, China (2023J05260); Major Science and Technology Projects by Natural Science Foundation of Fujian Province, China (No. 2022YZ035020); The Young Teachers Education Foundation of Fujian Province, China (No. JAT2200329); Innovation, Entrepreneurship, and Creation Education and Teaching Reform Research Project, Minjiang University (2022SCJG-03).

Ethics Statement: None

References

1. Turgut F, Awad AS, Abdel-Rahman EM. Acute kidney injury: medical causes and pathogenesis. J Clin Med. 2023;12(1):375. doi:10.3390/jcm12010375
2. Marx D, Metzger J, Pejchinovski M, Gil RB, Frantzi M, Latosinska A, et al. Proteomics and Metabolomics for AKI Diagnosis. Semin Nephrol. 2018;38(1):63–87. doi:10.1016/j.semnephrol.2017.09.007
3. Bellomo R, Kellum JA, Ronco C. Acute kidney injury. Lancet. 2012;380(9843):756–66. doi:10.1016/S0140-6736(11)61454-2
4. Chalkias A, Xanthos T. Acute kidney injury. Lancet. 2012;380(9857):1904. [author reply 1905]. doi:10.1016/S0140-6736(12)62104-7
5. Kumar S. Cellular and molecular pathways of renal repair after acute kidney injury. Kidney Int. 2018;93(1):27–40. doi:10.1016/j.kint.2017.07.030
6. Lin Q, Li S, Jiang N, Shao X, Zhang M, Jin H, et al. PINK1-parkin pathway of mitophagy protects against contrast-induced acute kidney injury via decreasing mitochondrial ROS and NLRP3 inflammasome activation. Redox Biol. 2019;26:101254. doi:10.1016/j.redox.2019.101254
7. Peerapornratana S, Manrique-Caballero CL, Gomez H, Kellum JA. Acute kidney injury from sepsis: current concepts, epidemiology, pathophysiology, prevention and treatment. Kidney Int. 2019;96(5):1083–99. doi:10.1016/j.kint.2019.05.026
8. Chen HZ, Busse LW. Novel therapies for acute kidney injury. Kidney Int Rep. 2017;2(5):785–799. doi:10.1016/j.ekir.2017.06.020
9. Martin-Sanchez D, Ruiz-Andres O, Poveda J, Carrasco S, Cannata-Ortiz P, Sanchez-Niño MD, et al. Ferroptosis, but not necroptosis, is important in nephrotoxic folic acid–induced AKI. J Am Soc Nephrol. 2017;28(1):218–29. doi:10.1681/ASN.2015121376
10. Liu D, Liang CH, Huang B, Zhuang X, Cui W, Yang L, et al. Tryptophan metabolism acts as a new anti-ferroptotic pathway to mediate tumor growth. Adv Sci (Weinh). 2023;10(6):e2204006. doi:10.1002/advs.202204006
11. Guo S, Zhou L, Liu X, Gao L, Li Y, Wu Y. Baicalein alleviates cisplatin-induced acute kidney injury by inhibiting ALOX12-dependent ferroptosis. Phytomedicine. 2024;130(2024):155757. doi:10.1016/j.phymed.2024.155757
12. Deng Y, Zeng L, Liu H, Zuo A, Zhou J, Yang Y, et al. Silibinin attenuates ferroptosis in acute kidney injury by targeting FTH1. Redox Biol. 2024;77:103360. doi:10.1016/j.redox.2024.103360
13. Li HD, Meng XM, Huang C, Zhang L, Lv XW, Li J. Application of herbal traditional Chinese medicine in the treatment of acute kidney injury. Front Pharmacol. 2019;10:376. doi:10.3389/fphar.2019.00376
14. Stepanić V, Kučerová-Chlupáčová M 2023. Review and chemoinformatic analysis of ferroptosis modulators with a focus on natural plant products.Molecules. 2023;28(2):475.
15. Tsuda T. Curcumin as a functional food-derived factor: degradation products, metabolites, bioactivity, and future perspectives. Food Funct. 2018;9(2):705–14. doi:10.1039/C7FO01242J
16. Zhao YH, Shen CF, Kang Y, Qi A, Xu WJ, Shi WH, et al. Curcumin prevents renal cell apoptosis in acute kidney injury in a rat model of dry-heat environment heatstroke via inhibition of the mitochondrial apoptotic pathway. Exp Ther Med. 2021;21(2):126. doi:10.3892/etm.2020.9558
17. Zhou J, Wu N, Lin L. Curcumin suppresses apoptosis and inflammation in hypoxia/reperfusion-exposed neurons via wnt signaling pathway. Med Sci Monit. 2020;26:e920445. doi:10.12659/MSM.920445

18. Gong X, Jiang L, Li W, Liang Q, Li Z. Curcumin induces apoptosis and autophagy inhuman renal cell carcinoma cells via Akt/mTOR suppression. Bioengineered. 2021;12(1):5017–27. doi:10.1080/21655979.2021.1960765
19. Awad AS, El-Sharif AA. Curcumin immune-mediated and anti-apoptotic mechanisms protect against renal ischemia/reperfusion and distant organ induced injuries. Int Immunopharmacol. 2011;11(8):992–6. doi:10.1016/j.intimp.2011.02.015
20. Afrin MR, Arumugam S, Rahman MA, Karuppagounder V, Harima M, Suzuki H, et al. Curcumin reduces the risk of chronic kidney damage in mice with nonalcoholic steatohepatitis by modulating endoplasmic reticulum stress and MAPK signaling. Int Immunopharmacol. 2017;49:161–7. doi:10.1016/j.intimp.2017.05.035
21. Ghelani H, Razmovski-Naumovski V, Chang D, Nammi S. Chronic treatment of curcumin improves hepatic lipid metabolism and alleviates the renal damage in adenine-induced chronic kidney disease in Sprague-Dawley rats. BMC Nephrol. 2019;20(1):431. doi:10.1186/s12882-019-1621-6
22. Kar F, Hacioglu C, Senturk H, Donmez DB, Kanbak G, Uslu S. Curcumin and LOXblock-1 ameliorate ischemia-reperfusion induced inflammation and acute kidney injury by suppressing the semaphorin-plexin pathway. Life Sci. 2020;256:118016. doi:10.1016/j.lfs.2020.118016
23. Wu T, Marakkath B, Ye Y, Khobahy E, Yan M, Hutcheson J, et al. Curcumin attenuates both acute and chronic immune nephritis. Int J Mol Sci. 2020;21(5):1745.
24. Zhu H, Wang X, Wang X, Liu B, Yuan Y, Zuo X. Curcumin attenuates inflammation and cell apoptosis through regulating NF-kappaB and JAK2/STAT3 signaling pathway against acute kidney injury. Cell Cycle. 2020;19(15):1941–51. doi:10.1080/15384101.2020.1784599
25. Dastani M, Rahimi HR, Askari VR, Jaafari MR, Jarahi L, Yadollahi A, et al. Three months of combination therapy with nano-curcumin reduces the inflammation and lipoprotein (a) in type 2 diabetic patients with mild to moderate coronary artery disease: evidence of a randomized, double-blinded, placebo-controlled clinical trial. Biofactors. 2023;49(1):108–18. doi:10.1002/biof.1874
26. Ramezani V, Ghadirian S, Shabani M, Boroumand MA, Daneshvar R, Saghafi F. Efficacy of curcumin for amelioration of radiotherapy-induced oral mucositis: a preliminary randomized controlled clinical trial. BMC Cancer. 2023;23(1):354. doi:10.1186/s12885-023-10730-8
27. Wei Z, Shaohuan Q, Pinfang K, Chao S. Curcumin attenuates ferroptosis-induced myocardial injury in diabetic cardiomyopathy through the Nrf2 pathway. Cardiovasc Ther. 2022;2022:3159717. doi:10.1155/2022/3159717
28. Jang C, Chen L, Rabinowitz JD. Metabolomics and Isotope Tracing. Cell. 2018;173(4):822–37. doi:10.1016/j.cell.2018.03.055
29. Johnson CH, Ivanisevic J, Siuzdak G. Metabolomics: beyond biomarkers and towards mechanisms. Nat Rev Mol Cell Biol. 2016;17(7):451–9. doi:10.1038/nrm.2016.25
30. Nicholson JK, Lindon JC, Holmes E. 'Metabonomics': understanding the metabolic responses of living systems to pathophysiological stimuli via multivariate statistical analysis of biological NMR spectroscopic data. Xenobiotica. 1999;29(11):1181–9. doi:10.1080/004982599238047
31. Konjevod M, Erjavec GN, Perkovic MN, Sáiz J, Tudor L, Uzun S, et al. Metabolomics in posttraumatic stress disorder: untargeted metabolomic analysis of plasma samples from Croatian war veterans. Free Radic Biol Med. 2021;162:636–41. doi:10.1016/j.freeradbiomed.2020.11.024
32. Konjevod M, Tudor L, Strac DS, Erjavec GN, Barbas C, Zarkovic N, et al. Metabolomic and glycomic findings in posttraumatic stress disorder. Prog Neuro Psychopharmacol Biol Psychiatry. 2019;88:181–93. doi:10.1016/j.pnpbp.2018.07.014
33. Li Q, Xing C, Yuan Y. Mitochondrial targeting of herbal medicine in chronic kidney disease. Front Pharmacol. 2021;12:632388. doi:10.3389/fphar.2021.632388
34. Hopkins AL. Network pharmacology. Nat Biotechnol. 2007;25(10):1110–1. doi:10.1038/nbt1007-1110
35. Hopkins AL. Network pharmacology: the next paradigm in drug discovery. Nat Chem Biol. 2008;4(11):682–90. doi:10.1038/nchembio.118
36. Tao C, Wang J, Gu Z, Ni H, Luo Y, Ling J, et al. Network pharmacology and metabolomics elucidate the underlying mechanisms of Venenum Bufonis in the treatment of colorectal cancer. J Ethnopharmacol. 2023;317:116695. doi:10.1016/j.jep.2023.116695

37. Mao T, Xie L, Guo Y, Ji X, Wan J, Cui X, et al. Mechanistic exploration of Yiqi Liangxue Shengji prescription on restenosis after balloon injury by integrating metabolomics with network pharmacology. Pharm Biol. 2023;61(1):1260–73. doi:10.1080/13880209.2023.2244533
38. Li T, Zhang W, Hu E, Sun Z, Li P, Yu Z, et al. Integrated metabolomics and network pharmacology to reveal the mechanisms of hydroxysafflor yellow A against acute traumatic brain injury. Comput Struct Biotechnol J. 2021;19:1002–13. doi:10.1016/j.csbj.2021.01.033
39. Wang Y, Quan F, Cao Q, Lin Y, Yue C, Bi R, et al. Quercetin alleviates acute kidney injury by inhibiting ferroptosis. J Adv Res. 2020;28:231–43. doi:10.1016/j.jare.2020.07.007
40. Jin J, Xu F, Zhang Y, Guan J, Liang X, Zhang Y, et al. Renal ischemia/reperfusion injury in rats is probably due to the activation of the 5-HT degradation system in proximal renal tubular epithelial cells. Life Sci. 2021;285:120002.
41. Hu Z, Zhang H, Yi B, Yang S, Liu J, Hu J, et al. VDR activation attenuate cisplatin induced AKI by inhibiting ferroptosis. Cell Death Dis. 2020;11(1):73. doi:10.1038/s41419-020-2256-z
42. Cai F, Li D, Zhou K, Zhang W, Yang Y. Tiliroside attenuates acute kidney injury by inhibiting ferroptosis through the disruption of NRF2-KEAP1 interaction. Phytomedicine. 2024;126:155407. doi:10.1016/j.phymed.2024.155407
43. Li W, Xiang Z, Xing Y, Li S, Shi S. Mitochondria bridge HIF signaling and ferroptosis blockage in acute kidney injury. Cell Death Dis. 2022;13(4):308. doi:10.1038/s41419-022-04770-4
44. Tang X, Ding H, Liang M, Chen X, Yan Y, Wan N, et al. Curcumin induces ferroptosis in non-small-cell lung cancer via activating autophagy. Thorac Cancer. 2021;12(8):1219–30. doi:10.1111/1759-7714.13904
45. Wu L, Dong B, Chen Q, Wang Y, Han D, Zhu X, et al. Effects of curcumin on oxidative stress and ferroptosis in acute ammonia stress-induced liver injury in gibel carp (Carassius gibelio). Int J Mol Sci. 2023;24(7):6441.
46. Abbasi S, Sato Y, Kajimoto K, Harashima H. New design strategies for controlling the rate of hydrophobic drug release from nanoemulsions in blood circulation. Mol Pharm. 2020;17(10):3773–82. doi:10.1021/acs.molpharmaceut.0c00542
47. Wu J, Pan X, Fu H, Zheng Y, Dai Y, Yin Y, et al. Effect of curcumin on glycerol-induced acute kidney injury in rats. Sci Rep. 2017;7(1):10114. doi:10.1038/s41598-017-10693-4
48. El-Gizawy MM, Hosny EN, Mourad HH, Abd-El Razik AN. Curcumin nanoparticles ameliorate hepatotoxicity and nephrotoxicity induced by cisplatin in rats. Naunyn Schmiedebergs Arch Pharmacol. 2020;393(10):1941–53. doi:10.1007/s00210-020-01888-0
49. Kumar P, Sulakhiya K, Barua CC, Mundhe N. TNF-alpha, IL-6 and IL-10 expressions, responsible for disparity in action of curcumin against cisplatin-induced nephrotoxicity in rats. Mol Cell Biochem. 2017;431(1–2):113–22. doi:10.1007/s11010-017-2981-5
50. Cao X, Li Y, Wang Y, Yu T, Zhu C, Zhang X, et al. Curcumin suppresses tumorigenesis by ferroptosis in breast cancer. PLoS One. 2022;17(1):e0261370. doi:10.1371/journal.pone.0261370
51. Chen M, Tan AH, Li J. Curcumin represses colorectal cancer cell proliferation by triggering ferroptosis via PI3K/Akt/mTOR Signaling. Nutr Cancer. 2023;75(2):726–33. doi:10.1080/01635581.2022.2139398
52. Cai Y, Huang C, Zhou M, Xu S, Xie Y, Gao S, et al. Role of curcumin in the treatment of acute kidney injury: research challenges and opportunities. Phytomedicine. 2022;104:154306. doi:10.1016/j.phymed.2022.154306
53. Feng T, Wei Y, Lee RJ, Zhao L. Liposomal curcumin and its application in cancer. Int J Nanomed. 2017;12:6027–44. doi:10.2147/IJN.S132434
54. Huang M, Liang C, Tan C, Huang S, Ying R, Wang Y, et al. Liposome co-encapsulation as a strategy for the delivery of curcumin and resveratrol. Food Funct. 2019;10(10):6447–58. doi:10.1039/C9FO01338E
55. Jardim KV, Siqueira JL, Bao SN, Sousa MH, Parize AL. The role of the lecithin addition in the properties and cytotoxic activity of chitosan and chondroitin sulfate nanoparticles containing curcumin. Carbohydr Polym. 2020;227:115351. doi:10.1016/j.carbpol.2019.115351
56. Shoba G, Joy D, Joseph T, Majeed M, Rajendran R, Srinivas PS. Influence of piperine on the pharmacokinetics of curcumin in animals and human volunteers. Planta med. 1998;64(4):353–6. doi:10.1055/s-2006-957450